Journal of Sound and Vibration (2000) **231**(3), 689–701
doi:10.1006/jsvi.1999.2647, available online at http://www.idealibrary.com on IDEAL®

HIGH-SPEED RAILWAY LINES ON SOFT GROUND: DYNAMIC BEHAVIOUR AT CRITICAL TRAIN SPEED

C. MADSHUS AND A. M. KAYNIA

Norwegian Geotechnical Institute, Sognsvn. 72, P.O. Box 3930 Ullevaal Stadion, N-0806 Oslo, Norway

(*Received in final form 23 September* 1999)

Results from instrumented test runs with a high-speed train on a soft soil site in Sweden are presented. It is shown that large dynamic amplifications appear in the dynamic response of the rail/embankment/ground system as the train speed approaches an apparently critical value. The measured dynamic response is analyzed in detail, and it is shown that the critical speed is controlled by the minimum phase velocity of the first Rayleigh mode of the soil and embankment profile at the site. Moreover, it is shown that the critical speed and the amount of dynamic amplification also depend on a coincidence between characteristic wavelengths for the site and the distances between bogies and axles in the train. The displacement response is found to consist of a speed-independent portion in quasi-static equilibrium with the train loads and a dynamic portion representing freely propagating Rayleigh waves. An efficient computer code for the prediction of ground response to high-speed trains has been developed and its ability to reproduce the observed behaviour is demonstrated.

1. INTRODUCTION

The fifth IWRN in Voss, 1995, clearly pointed out the increasing importance of ground vibration as part of the "Noise problem" of modern railway traffic. About 25% of the contributed papers dealt with this topic, and it attracted an even greater portion of the discussions. Models for vibration generation, propagation, response of structures and perception by humans were discussed on theoretical, empirical and numerical bases.

One topic which was not touched at Voss, and which has surfaced primarily in the last few years, is the problem of high-speed trains approaching the critical speed for the rail/embankment/ground system [1–8]. It was known as early as in 1927 [9] that a rail as a beam attached to the sleepers and elastically supported on the ballast should theoretically have a critical speed at which excessive dynamic amplification of the vertical motion during train passage should be expected. However, with commonly assumed properties of the subgrade stiffness this speed was estimated to be about 500 m/s [10], and thus far above any realistic train speed. More recently, it has been shown that trains may theoretically encounter another lower critical speed when reaching the Rayleigh wave velocity of the

0022-460X/00/130689 + 13 $35.00/0

ground [1]. The fact that a "resonance-like" condition appears when a moving line- or point-load reaches this speed had previously been shown through theory [11–14]. This phenomenon had also been observed for propagation of air pressure waves from blasts. The problem, however, appears to be more complicated than simply an interaction with the Rayleigh wave in the ground. The rail/embankment system behaves as a beam in dynamic interaction with the ground. Based on this assumption, it has been found [2, 3] that beams on a homogeneous half-space should have two critical speeds, one equal to the Rayleigh wave velocity of the ground, and the other, fairly close, controlled by the bending stiffness and mass of the rail/embankment "beam" in addition to the ground properties. Various approaches based on analytical wave equation solutions [2, 3], Green's functions [1, 6, 8], wavelets [7], boundary and finite elements, even with the element net moving with the train [4], have been applied to try to predict rail/embankment/ground response to trains passing at speeds around the critical value.

Development of high-speed train lines is growing rapidly throughout Europe, the far East and North America. Train speeds have increased from 200 to more than 300 km/h. The speed record on railed track exceeds 500 km/h. Demands on high train speeds and short travel time calls for straight lines which make the crossing of soft soil zones unavoidable. Peat, organic clays and soft marine clays may have a shear wave velocity, and thus a Rayleigh wave velocity, as low as 40–50 m/s. Problems with high-speed lines, and even traditional tracks, reaching the critical speed can therefore be expected to an increasing amount. Demands for safe lines, rapid construction and cost-effective solutions are becoming apparent. Observations by railway companies in France, Germany, Swiss, Holland and Great Britain of substantial increase in the vertical movement in the track as the train speed approaches the Rayleigh wave speed in the ground, have been cited in references [2,3]. Unfortunately, little data from the observations, analyses and validated predictions have so far been reported in the literature, and the severity of the problem does not seem to be widely known.

A recent test programme at a site in Sweden, where the critical speed problem was encountered, has provided a unique opportunity to measure the response of the rail/embankment/ground system. The data have been analyzed, dynamic properties of the site have been investigated, a computer code developed, validated and used for further prediction and physical interpretation of the phenomenon.

2. CRITICAL TRAIN SPEED OBSERVATIONS IN SWEDEN

2.1. INVESTIGATIONS PERFORMED

The Swedish National Rail Administration (Banverket) opened a service with the X-2000 high-speed train along their West Coast Line between Göteborg and Malmö early in 1997. Shortly after starting the service, excessive vibrations of the railway embankment, surrounding soil and overhead power-line pylons were detected at several soft soil locations during train passage at speeds of around 200 km/h. Questions were raised about the running safety of the trains, degradation

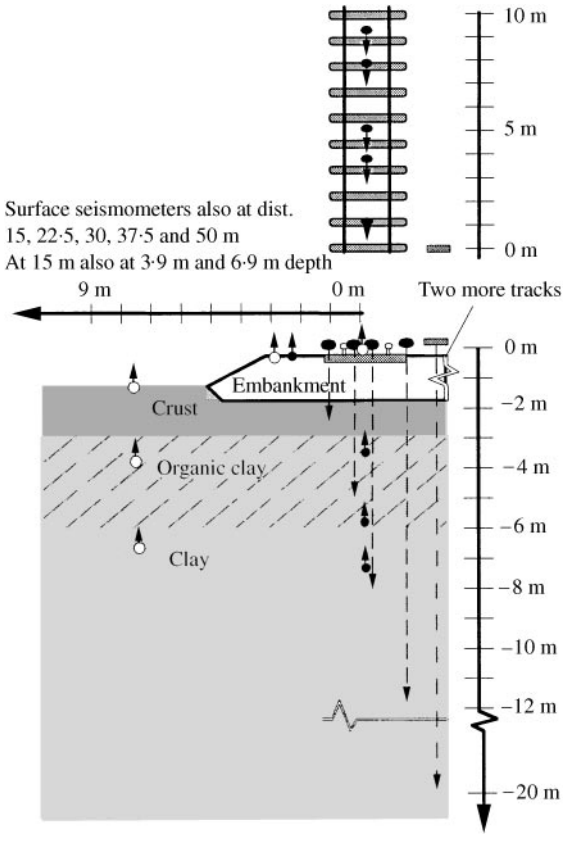

Figure 1. Test site and instrumentation: , Accelerometer; , Seismometer; , Electronic displacement sensor; , Video displacement sensor.

of the supporting soil, distoration of the embankment, fatigue failure in the rails, disruption of power supply to the trains and disturbing vibrations in the surroundings. As an immediate action, the train speed was reduced at the soft soil locations, and investigations were begun to diagnose the problem, quantify its extent and find solutions. As part of these investigations, extensive measurements of the dynamic response of the rail, embankment and soil were made at a selected site during the Autumn of 1997. Additional measurements of the ground and embankment properties were performed during the spring of 1998. Preliminary measurements of the response to passing high-speed trains have also been made at a nearby site on uniform marine clay.

Figure 1 shows a cross-section through the track and ground at the test site and a plan view. The ground at the site consists of a weathered clay crust and a layer of extremely soft organic clay over soft marine clays. The depth to bedrock is more than 65 m. Rail type is UIC60 on concrete sleepers at 0·67 m spacing. The embankment is about 1·4 m thick, made of crushed rock ballast, gravel and sand. Low and light embankments are often used on soft soil sites to reduce settlements. An X-2000 passenger train consisting of locomotive and four cars as illustrated in Figure 2(a) was used for the tests. The Figure also indicates the axle loads of the

train. A total of 20 test runs were made, with train speeds ranging from 10 to 202 km/h, in both northbound and southbound directions. In addition, two static tests with the train were performed. The train had its locomotive in front when northbound and at the rear when southbound.
Figure 1 also shows the instrumentation used; comprising:

(a) Four electronic sensors measuring the vertical displacement of sleepers relative to rods anchored in the ground at 2·4, 5, 8 and 12 m depths. Each sensor had an offset along the track as shown in the Figure.
(b) A reference rod anchored at 20 m depth, measuring the vertical displacement of the rail through video recording.
(c) Vertical and horizontal accelerometers at the top of the embankment and in the ground at 7·4, 5·4 and 3·4 m depths (varied throughout the test programme).
(d) Seismometers (particle velocity sensors) at the embankment and on the ground surface in a line perpendicular to the track at various distances out to 50 m from the track. At some positions seismometers were also installed in the ground at 3·9 and 6·9 m depths.

Overall good agreement was obtained between the results from the various measurement systems.

2.2. OBSERVED BEHAVIOUR

Figures 2(b) and 2(c) present examples of recorded time histories of vertical displacement. (b) is from a southbound train at 70 km/h, while (c) is from a northbound train at 185 km/h. To make the traces more easily comparable they are all plotted along a common space axis, converted from a time axis through multiplication by the train speed.
The following important observations can be made from these plots and corresponding plots from the rest of the recorded train passages (not presented here):

- The displacements increase drastically for increased train speed above a certain value.
- For train speeds below about 70 km/h the displacements appear as quasi-static. They are always directed downwards, are a "mirror image" of the axle loads and do not change with the train speed. The displacement pattern is symmetrical in time, except for the small non-symmetry in the train load pattern.
- For higher train speeds, displacements are both upwards and downwards. The displacement pattern is non-symmetrical in time with hardly any displacements ahead of the train but with a "tail" of "free oscillation" following the train.

Figure 3 is a summary of the downward and upward displacement peaks from all recorded train passages, plotted versus train speed. A thorough analysis of the recorded data reveals that the displacement pattern, both at the embankment and in the ground can be decomposed into two fields:

- A quasi-static displacement field, whose corresponding stress field is in static equilibrium with the surface loads from the train. This field moves with the train,

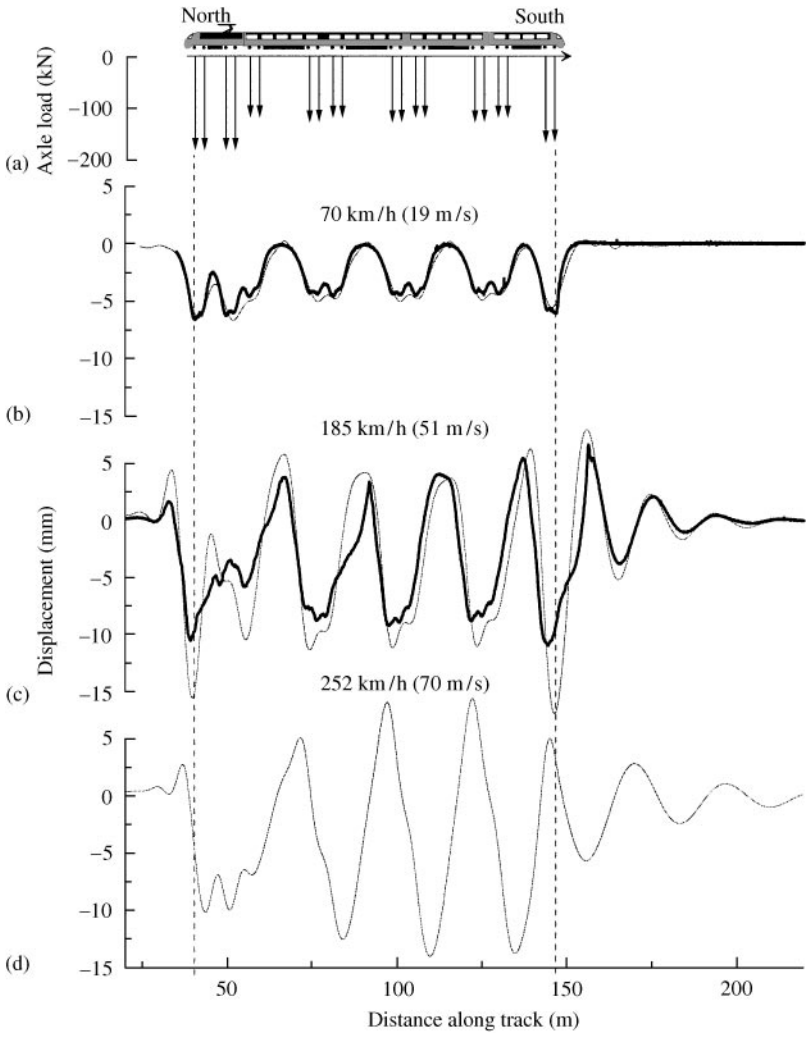

Figure 2. Train geometry and loads. Measured and simulated vertical displacement response: ——, Measured, ---, Simulated.

and its pattern and amplitudes do not change with the train speed. The field contains only downward motions.

- A dynamic displacement field associated mainly with Rayleigh waves in the rail/embankment/ground system. The corresponding internal stresses are in dynamic equilibrium without any additional surface loads. This field has equal upward and downward displacement amplitudes. Its pattern is non-symmetrical in time, with a rapid build up under the first part of the train and a decay behind the train. The propagation speed of this field in the direction of the train motion is identical to the train speed.

Both displacement fields appear to follow the train motion and will thus be stationary, relative to the train.

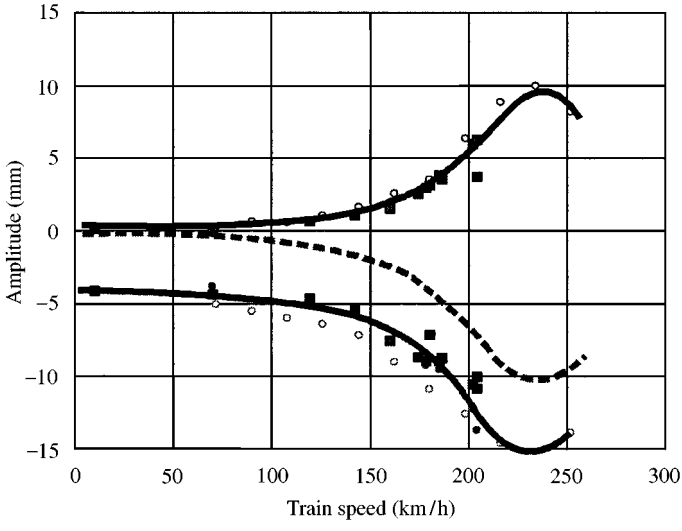

Figure 3. Displacement amplitude versus train speed: measured and simulated: ■, Measured-Displacement transducer; ▬, Measured-Accelerometer; ○, Simulated; ———, Best-fit line, total displacement, −−, Best fit line, isolated dynamic ampl.

Figure 3 also plots the amplitude of the isolated dynamic embankment displacements versus train speed. It appears that for this test site, a speed of about 70 km/h appears as a "cut-off speed" below which no waves are generated. Above 70 km/h, waves are generated and their dynamic amplification increases rapidly for increased train speed. 202 km/h was the highest speed which could be reached during the tests. The trend indicates that the displacements may increase still further for increases in train speed. Analysis presented later will show that the maximum response should be expected at about 235 km/h, which may appear as a "critical speed" for this train and site.

Analysis of the decaying oscillation tail which follows the train, when it runs faster than the cut-off speed, have revealed that

— its phase velocity along the embankment matches the train speed
— its frequency is independent of the train speed, and for this site is 2·7 Hz.
— its apparent "damping" determined from its decay rate is between 20 and 30%.

Further theoretical studies have revealed that indeed these properties are features belonging to the dynamic deformation field. These analyses prove that the oscillating tail should be stationary relative to the train.

3. INTERPRETATION AND NUMERICAL SIMULATION

3.1. SITE-SPECIFIC PROPERTIES

To enable further interpretation and numerical simulations, the properties of soil and embankment materials at the site were thoroughly mapped. Penetration

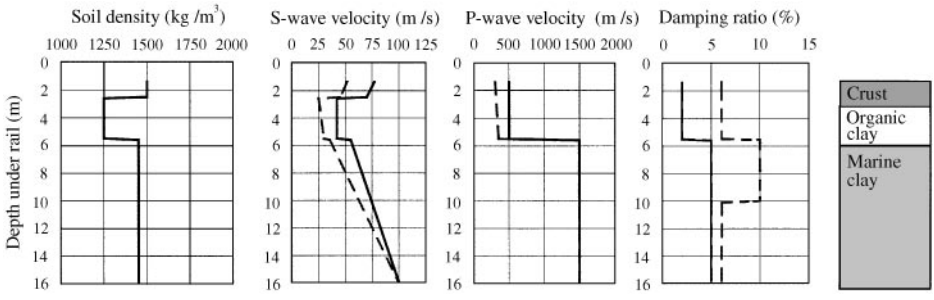

Figure 4. Dynamic soil parameters for test site. ——, Small strain values, "Initial"; – –, values accounting for non-linearity.

testing and sampling was used to determine the soil layering, classify the soil types and resolve key parameters. Cross-hole, down hole and SASW (Spectral Analyses of Surface Waves) seismic methods [15, 16] were used for *in situ* determination of wave velocities in the soil and embankment. In addition, dynamic (cyclic) triaxial tests (with piezo-bender velocity measurements included) were performed on undisturbed samples from the site [17, 18]. Figure 4 summarizes (solid lines) established mass density, shear wave velocity, compressional wave velocity and damping versus depth for the soil profile at the site. One should particularly observe the soft layer of organic clay with a shear wave velocity about 40 m/s. The depth scale in the figure refers to the top of the embankment.

The 1·4 m deep embankment has an average mass density of 1800 kg/m^3, a shear wave velocity of 250 m/s and a compressional wave velocity of 470 m/s.

Analysis of recorded train-induced displacements reveal that dynamic strains in the ground and embankment for high-speed train passages are so high that the materials behave nonlinearly. Figure 5(a) shows a typical non-linear hysteresis loop for a soil material. In this project an "equivalent linear" approach is used, where the real hysteretic behaviour is approximated by introducing a reduced secant shear modulus and an increased hysteretic damping compared to the values determined for much lower strains by the seismic test. Dynamic triaxial laboratory tests were used to determine the modulus reduction and damping increase as a function of the strain-level for the materials. Figures 5(b) and 5(c) plot the determined modulus reduction and damping curves for the soil and embankment materials. By using these curves and strains estimated from the measured displacements during the train passages, best estimate equivalent linear material parameters have been determined, as plotted also in Figure 4 (dotted lines). For the embankment material, the non-linearity at the highest train speeds leads to a reduction of the wave speeds to 150 and 220 m/s for shear and compression, respectively, and to a hysteretic damping of about 13%.

3.2. COMPUTER PROGRAM

A computer program, VibTrain, has been developed to simulate and analyze the response of rail/embankment/ground systems to high-speed train passage. The

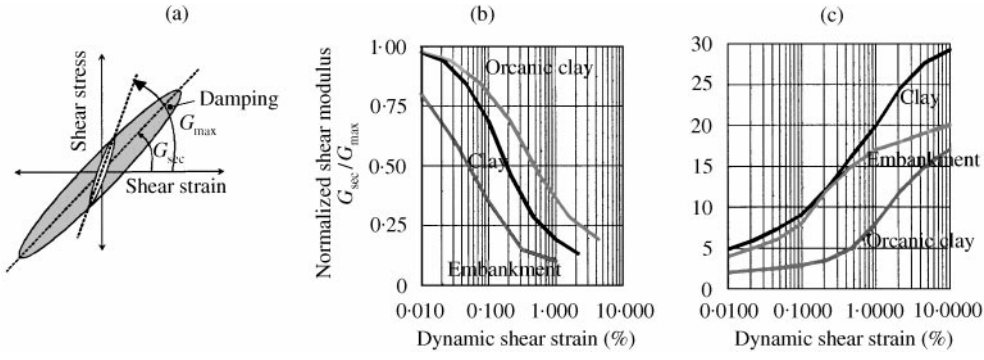

Figure 5. Non-linearity of soil and embankment materials: equivalent linear approach.

program is based on substructuring, whereby the ground is represented by discrete Green's functions for layered half-space [19], and the rail/embankment system is represented as a beam by finite elements. The two systems are connected through a series of coupling points along the ground surface under the embankment, where compatibility in vertical displacement and stress are enforced. Green's functions are used to derive a dynamic flexibility matrix for the coupling points at the ground surface. This is inverted to a stiffness matrix and added to the stiffness matrix of the rail/embankment system. The train loads, as presented in Figure 2(a) are applied to the nodal points of the beam, which coincide with the sleeper positions. The train motion is obtained by appropriately delaying the loads from point to point according to the train speed. To avoid the unnecessary extra computational efforts due to high frequencies, the bridging effect from the rails is inherently accounted for in the load application by smoothly distributing each bogie load over a 6 m span. All computations are made in the frequency domain. Response time-histories are obtained by an inverse Fourier transformation. The computational scheme is efficient; when the system of equations is established and solved for a site, each response calculation is limited to a matrix multiplication and the inverse Fourier transform. See reference [20] for a more detailed account of the model.

3.3. RESULTS, VALIDATION AND PREDICTIONS

Figures 2(b)–(d) plot the computed vertical displacement response time-history for trains at speeds 70, 185 and 252 km/h. For the first two train speeds actual measurements were made during the tests with X-2000 (shown in bold line). The good agreement which can be observed between computation and measurement, where all main features are reproduced, provides confidence that the program is adequate. The 252 km/h case (d) is an example of pure prediction for higher speed that could be reached during the tests. Figure 3 plots the computed upward and downward displacement amplitudes versus train speed together with the measured values. The good agreement is confirmed for all train speeds. According to the numerical predictions, the response should be expected to have a maximum for

train speed of about 235 km/h, and decrease for further increase in the speed. 235 km/h appears the most critical speed for this train at the test site.

It should be observed that for train speeds below critical, the downward displacement peaks roughly coincide with the instantaneous position of the train bogies. For speeds above critical, the vertical displacements appear to be about 180° out-of-phase with the bogie-loads towards the end of the train, where a "resonance-like" condition may have developed. Indications of a similar behaviour have been observed through preliminary measurements at the uniform clay site close to the test site. When close to the critical speed, bogie loads are about 90° ahead of the downward displacement peaks. Displacements out-of-phase with the loads may have a large effect on the dynamic interaction between train and rail/embankment, and may affect rolling resistance and the generation of ground vibrations.

The computer code has also been used to study the natural frequency and damping properties when the rail/embankment/ground system is excited by stationary harmonic loads. An apparent natural frequency of 2·4 Hz with 30% damping was found. In addition, free wave propagation along the embankment from performed impact test was simulated. Waves at 2·3 Hz travelling with phase velocity 51 m/s were found to dominate.

4. PHYSICAL INTERPRETATION

The rail/embankment/ground response to high-speed trains is easier to understand when viewed in the frequency–wave number ($\omega - k$) domain than in the time–space domain. Here the response $R(\omega, k)$ can be expressed as the product:

$$R(\omega, k) = H(\omega, k) \cdot P(\omega, k),$$

where $H(\omega, k)$ is a site-specific dynamic transfer function and $P(\omega, k)$ is the train load excitation function.

Figure 6(a) illustrates the magnitude of $H(\omega, k)$ for the actual test site in a three-dimensional contour plot. The ridge in ω–k space (dotted curve) which forms the locus where $H(\omega, k)$ and thus the dynamic amplification has its highest values, follows the dispersion curve for the first Rayleigh mode of the soil/embankment profile of the test site, as presented in Figure 4. It appears, as expected, that on this locus the points corresponding to free propagating waves from the simulated drop tests and the natural frequency of the rail embankment/ground system found for stationary excitation are also found. Also, the free oscillating displacement tails observed behind the trains during the tests are close to this locus. The steepest tangent through the origin to the dispersion curve defines the slowest Rayleigh wave possible at this site. Its phase velocity is 51 m/s. The hatched region in the upper left part of the ω–k plane is the quasi-static region. Moving loads here will not set-up waves, but only give quasi-static displacements. The border between this region and the "dynamic region" is the locus of the "cut-off speeds". Observe that although construction of $H(\omega, k)$ is a straightforward operation using a suitable numerical model (such as VibTrain explained in this

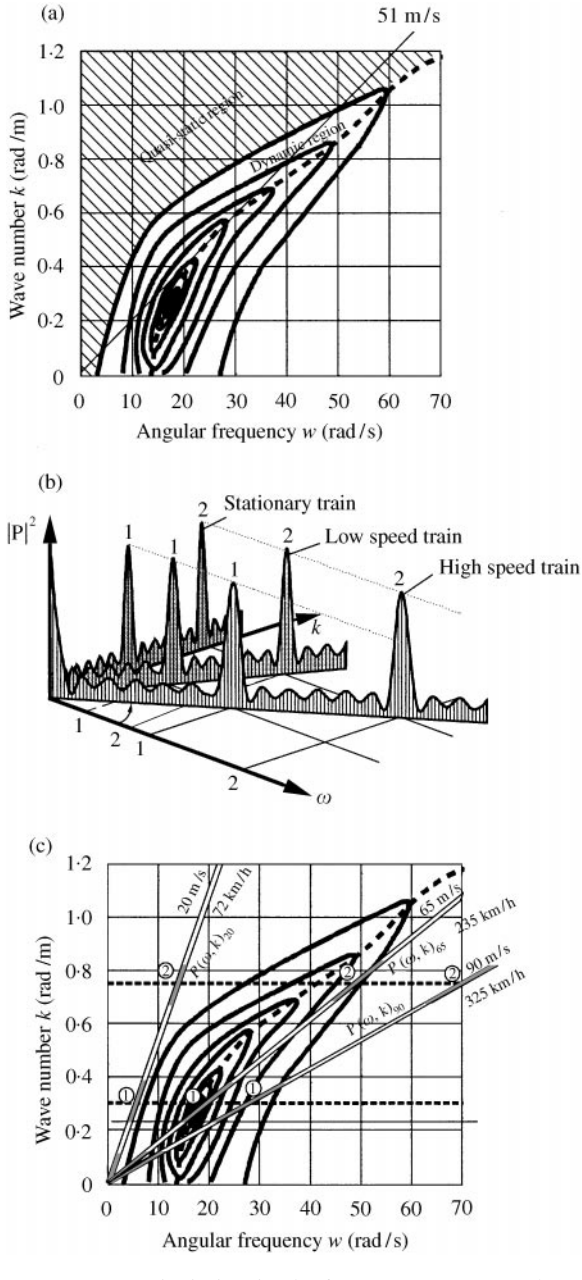

Figure 6. Response calculation in the frequency wave number domain.

paper), the plotted $H(\omega, k)$-function is only a schematic representation and is meant as an illustration of the response features.

The train load excitation function $P(\omega, k)$ is formed from the Fourier transform, $P(k)$, of the load sequence $p(x)$, shown in Figure 2. When the train moves at speed, S, $P(\omega, k)$ becomes

$$P(\omega, k) = P(k) \cdot \delta(k - 1/s \cdot \omega),$$

where δ is the Dirac Delta function. Figure 6(b) illustrates $P(\omega, k)$ for the X-2000 train when stationary, at a low speed and a high speed. The marked peaks in the function correspond to wavelengths equal to the distances between the main loads in the train, i.e., the longer bogie distances, the shorter bogie distance, etc. Other trains will have their peaks at other wavelengths, and when moving, at other frequencies.

In Figure 6(c), load functions $P(\omega, k)$ which were shown in three-dimensional view in Figure 6(b) are seen projected onto the ω–k plane for three train speeds 72, 235 and 325 km/h. They thus appear as straight lines. The ω–k regions where the $P(\omega, k)$-functions had their main peaks are visualized in Figure 6(c) by shading the lines in these regions. Figure 6(c) illustrates how $P(\omega, k)$ and the $H(\omega, k)$ from Figure 6(a) are multiplied to form the response $R(\omega, k)$. As shown, $R(\omega, k)$ derives contribution only along the line $k = 1/s \cdot \omega$, since $P(\omega, k)$ has values only here and is zero elsewhere. From the Figure it can be observed that for low train speeds, i.e., around 70 km/h and below, no dynamic amplification takes place, since $P(\omega, k)$ falls entirely in the quasi-static region of $H(\omega, k)$. For increased speed, the first and then the second peak in $P(\omega, k)$ starts to enter into the dynamic region of $H(\omega, k)$ and the response $R(\omega, k)$ starts to gain dynamic amplification. The response has its maximum at about 235 km/h (65 m/s) where the first and largest peak in $P(\omega, k)$ nearly coincides with the peak in $H(\omega, k)$. Further increase in train speed brings the peaks in $P(\omega, k)$ out of the regions where $H(\omega, k)$ gives high dynamic amplification, and the response will thus decrease for further increased train speed.

Figure 6 illustrates the important fact that a given site does not have one unique critical speed. Which speed is the most critical depends on the characteristic bogie and axle distances of the train relative to the dynamic transfer properties of the site, and may therefore vary among different trains. For example, note that for the X-2000 train and the actual test site in Figure 6(c) the lowest Rayleigh wave phase velocity, 51 m/s, is not the critical speed, since it does not lead to a coincidence between peaks in $H(\omega, k)$ and $P(\omega, k)$. The peaks are closest and the response reaches its maximum at about 235 km/h. Also note that the amount of dynamic amplification at the most unfavourable speed may be different for different trains.

5. CONCLUSIONS

It has been observed through measurements that large dynamic amplifications appear in the response of a rail/embankment/ground system when trains pass at speeds which approach an apparent critical value. The dynamic response has been measured and analyzed in detail. It is shown that the critical speed is controlled by the dispersion curve of the first Rayleigh mode of the soil and embankment profile at the site and the load distances of the train. The amount of dynamic amplification depends on the degree of coincidence between the characteristic wavelengths for the site and these load distances. The response displacement field is found to be stationary with respect to the moving train, and to be composed of two portions; one quasi-static in equilibrium with the train loads and another dynamic representing freely propagating Rayleigh waves. The quasi-static amplitudes do not

change with train speed, while the dynamic amplitudes increase drastically as the speed approaches critical. Below critical speed the displacements are in phase with the train loads: above critical they are of opposite phase.

ACKNOWLEDGMENTS

The authors wish to acknowledge the Swedish National Rail Administration (Banverket) for conducting and financing the presented project, and in particular Peter Zackrisson from their Headquarters for his excellent project management. We also thank Banverket for permitting the authors to release results from the project for publication. We wish to acknowledge the efforts of the rest of the project team; Kent Adolfson and Göran Wallmark from the Banverket Regional office, Per-Evert Benktsson from Swedish Geotechnical Institute, Anders Bodare from Royal Institute of Technology, Rainer Massarch from Geo Engineering AB, Bo Andréasson from Jacobson & Widemark AB and numerous co-workers from the various participating organizations.

REFERENCES

1. V. V. Krylov 1995 *Applied Acoustics* **44**, 149–164. Generation of ground vibrations by superfast trains.
2. H. A. Dieterman and A. V. Metrikine 1997 *European Journal of Mechanics, A/Solids* **16**, 295–306. Steady state displacements of a beam on an elastic half-space due to uniformly moving constant load.
3. A. R. M. Wolfert, H. A. Dieterman and A. V. Metrikine 1997 *Journal of Sound and Vibration* **203**, 597–606. Passing through the "elastic wave barrier" by a load moving along a waveguide.
4. C. Esveld and A. W. M. Kok 1997 *Post-Doctoral Course on High Speed Track, Technische Universitet Delf*, June 1997, 28p. Dynamic behaviour of railway track.
5. R. F. Woldrigh 1997 *PAO Course* "*High Speed Track*", Delft 11th June 1997, 7p. Notes on low embankments for high-speed lines on compressible subsoil.
6. V. V. Krylov 1998 *ACOUSTICA acta acostaica* **84**, 78–90. Effects of track properties on ground vibrations generated by high-speed trains.
7. M. Lieb and B. Sudret 1998 *Archive of Applied Mechanics* **68**, 147–157. A fast algorithm for soil dynamics calculation by wavelet decomposition.
8. V. V. Krylov 1998 *The Acoustic Bulletin* July/August 1998, 15–22. Ground vibration boom from high speed train: prediction and reality.
9. S. Timoshenko 1927 *Proceedings of the Second International Congress on Applied Mechanics*, Zurich, 1927. Methods of analysis of statical and dynamical stresses in rail.
10. C. Esveld 1989 *Graphic Department of Tyssen Stahl AG*, ISBN 90-800324-1-7, 446p. Modern railway track.
11. J. T. Kenney Jr 1954 *Journal of Applied Mechanics* **2**, 359–364. Steady state vibrations of beam on elastic foundation for moving load.
12. L. Frýba 1973 *Noordhoof International Publishing*. Groningen, ISBN 90 01, 48p. Vibrations of solids and structures under moving loads.
13. H. Werke and G. Waas 1987 *Soil Dynamics and Earthquake Engineering* **6**, 194–202. Analysis of ground motion caused by air pressure waves.
14. F. C. P. DeBarros and J. E. Luco 1994 *Wave Motion* **19**, 189–210. Response of a layered viscoelastic half-space to a moving point load.

15. R. D. Woods 1994 *Geophysical Characterisation of Sites* (R. D. Woods, editor), special volume of ISSMFE: TC10, New Delhi. Oxford & IBH Publishing Co, 91–100. Borehole methods in shallow seismic exploration.
16. K. H. Stokoe, S. G. Wright, J. A. Bay and J. M. Roësset 1994 R. D. Woods, editor, special Vol. of ISSMFE: TC10, 15–25. New Delhi: Oxford & IBH Publishing Co. Characterisation of geotechnical sites by SASW method geophysical characterization of sites.
17. R. Dyvik and C. Madshus 1985 *Proceedings of the ASCE Convention in Detroit, Michigan, October* 1985 (V. Kosla editor), 186–196. Lab. measurements of G_{max} using bender elements.
18. K. H. A. Andersen, A. Kleven and D. Heien (1988) *Journal of Geotechnical Engineering ASCE* **114**. Cyclic data for design of gravity structures.
19. E. Kausel and J. M. Roesset 1981 *Bulletin of the Seismological Society of America* **71**, 1743–1761. Stiffness matrices for layered soil.
20. A. M. Kaynia, C. Madshus and P. Zackrisson (in press) *Journal of Geotechnical and Geoenvironmental Engineering*, ASCE. Ground vibration from high speed trains:prediction and countermeasure.